PNAS RESEARCH ARTICLE | NEUROSCIENCE

TRPC4 and GIRK channels underlie neuronal coding of firing patterns that reflect $G_{q/11}$–$G_{i/o}$ coincidence signals of variable strengths

Jin-bin Tian[a,1], Jane Yang[b,c], William C. Joslin[a], Veit Flockerzi[d], Steven A. Prescott[b,c,e], Lutz Birnbaumer[f,g,1], and Michael X. Zhu[a,1]

Contributed by Lutz Birnbaumer; received November 16, 2021; accepted March 30, 2022; reviewed by Arthur Konnerth, Eve Marder, and Bernd Nilius

Transient receptor potential canonical 4 (TRPC4) is a receptor-operated cation channel codependent on both the $G_{q/11}$–phospholipase C signaling pathway and $G_{i/o}$ proteins for activation. This makes TRPC4 an excellent coincidence sensor of neurotransmission through $G_{q/11}$- and $G_{i/o}$-coupled receptors. In whole-cell slice recordings of lateral septal neurons, TRPC4 mediates a strong depolarizing plateau that shuts down action potential firing, which may or may not be followed by a hyperpolarization that extends the firing pause to varying durations depending on the strength of $G_{i/o}$ stimulation. We show that the depolarizing plateau is codependent on $G_{q/11}$-coupled group I metabotropic glutamate receptors and on $G_{i/o}$-coupled γ-aminobutyric acid type B receptors. The hyperpolarization is mediated by $G_{i/o}$ activation of G protein–activated inwardly rectifying K^+ (GIRK) channels. Moreover, the firing patterns, elicited by either electrical stimulation or receptor agonists, encode information about the relative strengths of $G_{q/11}$ and $G_{i/o}$ inputs in the following fashion. Pure $G_{q/11}$ input produces weak depolarization accompanied by firing acceleration, whereas pure $G_{i/o}$ input causes hyperpolarization that pauses firing. Although coincident $G_{q/11}$–$G_{i/o}$ inputs also pause firing, the pause is preceded by a burst, and both the pause duration and firing recovery patterns reflect the relative strengths of $G_{q/11}$ versus $G_{i/o}$ inputs. Computer simulations demonstrate that different combinations of TRPC4 and GIRK conductances are sufficient to produce the range of firing patterns observed experimentally. Thus, concurrent neurotransmission through the $G_{q/11}$ and $G_{i/o}$ pathways is converted to discernible electrical responses by the joint actions of TRPC4 and GIRK for communication to downstream neurons.

neurotransmission | coincidence detection | G proteins | neuronal firing | TRP channels

Significance

Neurons communicate by releasing neurotransmitters, many of which act at G protein–coupled receptors. Although it is well known that $G_{q/11}$ accelerates action potential firing while $G_{i/o}$ inhibits firing, how firing patterns change in response to simultaneous activation of $G_{q/11}$ and $G_{i/o}$ remains elusive, especially because the relative strength of $G_{q/11}$ versus $G_{i/o}$ activation varies greatly from event to event. This study reveals that neurons encode distinct messages that reflect coincident $G_{q/11}$ and $G_{i/o}$ stimulation by activating two ion channels, TRPC4 and GIRK. The resulting firing patterns, composed of burst, pause, and firing recovery phases, reflect both the occurrence of coincident $G_{q/11}$ and $G_{i/o}$ activation and their relative strengths. With these, we may begin to interpret the language of neurons.

In a neural network, neurons receive multiple transmitter inputs from the same or different regions that overlap in time. The encoded temporal information is incorporated in the output signals through concerted actions of receptors and ion channels. Among them, the vast number of G protein–coupled receptors signal through heterotrimeric G proteins to alter neuronal function via a limited set of effectors, including G protein–activated and/or receptor-operated channels capable of regulating excitability. However, in contrast to the rich knowledge on ionotropic receptors, the electrical responses induced by G protein signaling on postsynaptic neurons have not received as much attention. The widespread view that $G_{q/11}$ is excitatory while $G_{i/o}$ is inhibitory (1, 2) and that these signals are independent from one another is a gross oversimplification. Particularly, the $G_{q/11}$ and $G_{i/o}$ signaling pathways may be simultaneously activated by a neurotransmitter acting at two different receptor subtypes or by corelease of two or more neurotransmitters, each activating a unique G protein pathway. How a neuron processes coincident $G_{q/11}$ and $G_{i/o}$ inputs to produce discernible electrical responses remains mysterious.

At least two ion channels are coregulated by $G_{q/11}$ and $G_{i/o}$ pathways. First, G protein–activated inwardly rectifying K^+ (GIRK) channels are activated by $G_{i/o}$ but inhibited by $G_{q/11}$ because of their dependence on phosphatidylinositol 4,5-bisphosphate (PIP_2), a phospholipid hydrolyzed by phospholipase C (PLC) following $G_{q/11}$ activation (3–5). Second, the nonselective cation channel transient receptor potential canonical 4 (TRPC4) is codependent on both $G_{i/o}$ and PLC for activation (6–8). Although in the absence of $G_{i/o}$, such as when pertussis toxin (PTX) is applied to suppress $G_{i/o}$ function, the stimulation of $G_{q/11}$-coupled receptors can still very weakly evoke TRPC4 currents, the costimulation of $G_{i/o}$ evokes far more robust current (6). Thus, while the coincident activations of $G_{i/o}$ and $G_{q/11}$ antagonize each other at GIRK, they synergize to induce robust TRPC4 activation. Another distinction is that whereas GIRK activation is linked to hyperpolarization, TRPC4 activation causes depolarization.

Author contributions: J.-b.T., S.A.P., and M.X.Z. designed research; J.-b.T., J.Y., W.C.J., and S.A.P. performed research; V.F. and L.B. contributed new reagents/analytic tools; J.-b.T., J.Y., S.A.P., and M.X.Z. analyzed data; and J.-b.T., J.Y., S.A.P., L.B., and M.X.Z. wrote the paper.

Reviewers: A.K., Technische Universität München; E.M., Brandeis University; and B.N., Retired.

The authors declare no competing interest.

[1]To whom correspondence may be addressed. Email: jin.bin.tian@uth.tmc.edu, birnbau1@gmail.com, or michael.x.zhu@uth.tmc.edu.

This article contains supporting information online at http://www.pnas.org/lookup/suppl/doi:10.1073/pnas.2120870119/-/DCSupplemental.

Published May 11, 2022.

TRPC4-mediated electrical responses have been characterized in rodent lateral septal (LS) neurons (9, 10). As an important information processing center within the cerebrum, with connections to multiple areas of the forebrain and brainstem (11–14), the lateral septum receives inputs from many brain regions, including the hippocampus, prefrontal cortex, hypothalamus, amygdala, raphe nuclei, and ventral tegmental area, which release diverse neurotransmitters, such as acetylcholine, dopamine, glutamate, γ-aminobutyric acid (GABA), serotonin, and somatostatin, onto LS neurons (11–13, 15). Being mainly GABAergic neurons themselves, the LS neurons also communicate with each other via GABA (11, 16). Moreover, TRPC4 represents the most abundant TRPC isoform expressed in the lateral septum, at least at the mRNA level (17). It was reported that electrical stimulation of fimbria–fornix (fi–fx) fibers, which mediate excitatory inputs from the hippocampus to the LS (11, 18–20), elicited postsynaptic responses containing both glutamatergic and GABAergic components in LS neurons (11, 20). Among them, the $G_{q/11}$-coupled group I metabotropic glutamate receptors (mGluR1/5) appeared to underlie a depolarizing plateau potential that responded to electrical stimulation in the presence of blockers for ionotropic GABA and glutamate receptors (11, 21). In voltage clamp recordings, a large inward cation current activated by the mGluR1/5 agonist (1*S*,3*R*)-1-aminocyclopentane-1,3-dicarboxylic acid (ACPD) at resting or hyperpolarized potentials (e.g., −70 mV) is believed to underlie the depolarizing plateau (22, 23). These responses are more evident under conditions when ACPD was continuously superfused on the brain slice while LS neurons were intermittently depolarized by brief current injections, and they were later attributed to TRPC1–TRPC4 heteromeric channels (9, 21).

We previously showed that with a brief (30-ms) focal ejection of another mGluR1/5 agonist (*S*)-3,5-dihydroxyphenylglycine (DHPG) onto dendrites or somata, the majority of LS neurons in slices from wild-type (WT) mice also responded with the initial burst followed by a depolarizing plateau potential, which we coined above threshold plateau depolarization (ATPD). Cells that failed to develop ATPD exhibited a small (1 to 5 mV) depolarization of ∼3 to 8 s, which was named below threshold depolarization (BTD). Importantly, neither ATPD nor BTD was detected in LS neurons from *Trpc4*$^{-/-}$-mutant mice (10). Corresponding to the ATPD and BTD, TRPC4-dependent inward currents of large (0.2 to 1.6 nA) and small (<50 pA at −70 mV) amplitudes, respectively, were also detected in voltage clamp recordings (10), demonstrating the bipartite responses of mGluR-mediated TRPC4 activation. These are reminiscent of the large and small TRPC4 currents elicited by costimulating $G_{q/11}$–$G_{i/o}$ together and activating only $G_{q/11}$, respectively, in heterologous systems (6). Here, we show that ATPD is indeed dependent on the coactivation of $G_{q/11}$ and $G_{i/o}$ signaling no matter if it is triggered by electrical stimulation of fi–fx fibers or by direct application of receptor agonists. Additionally, we uncover how information about coincident $G_{q/11}$–$G_{i/o}$ inputs of varying strengths is encoded by neurons using action potential (AP) firing patterns shaped by TRPC4 and GIRK channels.

Results

Electrical Stimulation of Fi–Fx Fibers Generates Both TRPC4-Dependent Plateau Depolarization and TRPC4-Independent Hyperpolarization in LS Neurons. To test if ATPD occurs in LS neurons in response to neurotransmitters released by electrical stimulation, we applied a field stimulation protocol at fi–fx fibers in brain slices while the LS neuron was recorded under whole-cell current clamp with the baseline (prestimulus) potential adjusted to −45 mV (Fig. 1 *A* and *B*). Because LS neurons are mainly GABAergic and interconnected (11), the fi–fx fiber stimulation caused release of not only glutamate but also GABA. Although secondary, the GABA input was dominant under conditions of field electrical stimulation due to simultaneous activation of a large number of neighboring LS neurons by the fi–fx fibers. Thus, in the absence of fast synaptic blockers, only hyperpolarization was detected (*SI Appendix*, Fig. S1*A*). Although blocking $GABA_A$ receptors ($GABA_A$Rs) with bicuculline (10 μM) allowed a depolarizing plateau to occur (*SI Appendix*, Fig. S1 *B*, *Left*), the low success rate (37.5%, 3/8 WT neurons) and the presence of fast excitatory postsynaptic potential (fEPSP), as clearly seen in *Trpc4*$^{-/-}$ neurons (*SI Appendix*, Fig. S1 *B*, *Right*), precluded an accurate assessment of if the response represented ATPD and whether it was TRPC4 dependent. By including a subthreshold concentration of DHPG (1.3 μM), which was unable to induce ATPD on its own (10) or in combination with the fi–fx fiber stimulation (*SI Appendix*, Fig. S1*C*), the success rate reached 77.8% (7/9 WT neurons) (*SI Appendix*, Fig. S1 *D* and *E*), presumably due to the slight enhancement of extrasynaptic mGluR1/5 activation. However, with the additional application of cyanquixaline (6-cyano-7-nitroquinoxaline-2,3-dione) (CNQX, 15 μM) and D-2-amino-5-phosphonovalerate (D-AP5, 30 μM) to block fEPSPs, no depolarizing response was detected in all neurons tested (*SI Appendix*, Fig. S1*F*), indicating that the excitatory drive from α-amino-3-hydroxy-5-methyl-4-isoxazolepropionic acid (AMPA) and N-methyl-D-aspartic acid (NMDA) receptors was also important. To compensate for the loss of the excitatory drive, we added 4-aminopyridine (4-AP; 1 mM) in the perfusate to dampen the inhibitory drive from 4-AP–sensitive K^+ channels (*SI Appendix*, Fig. S1*G*). The addition of 4-AP restored the electrical stimulation–evoked depolarizing plateau in 50% (7/14) of WT LS neurons (Fig. 1 *B–D*), which shared similar amplitude and duration as ATPD induced by focal ejection of DHPG (10). The complete lack of such response in *Trpc4*$^{-/-}$ LS neurons (Fig. 1 *B–D*) also supported that the depolarizing plateau most likely derived from TRPC4 and thus represented ATPD.

However, different from ATPD induced by focal ejection of DHPG, the electrical stimulation–evoked ATPD was often followed by a hyperpolarization (Fig. 1*B*). A hyperpolarization was also detected in WT neurons that did not develop ATPD, and in the majority of *Trpc4*$^{-/-}$ neurons, neither its amplitude nor its duration differed between WT and *Trpc4*$^{-/-}$ neurons (Fig. 1 *E* and *F*) nor were there differences between WT neurons that displayed ATPD and those that did not (amplitude, $P = 0.965$; duration, $P = 0.276$; data points shown in Fig. 1 *E* and *F*). Since $GABA_A$Rs were blocked by bicuculline, we focused on $GABA_B$ receptors ($GABA_B$Rs). Previously, $GABA_B$Rs and a K^+ channel were implicated in the fi–fx fiber stimulation–evoked hyperpolarization in LS neurons, which was also sensitive to PTX (11, 24). Consistently, both CGP55845, a $GABA_B$R blocker, and tertiapin-Q, a GIRK channel inhibitor, suppressed the hyperpolarization (*SI Appendix*, Fig. S2 *A* and *B*). Thus, the robust GABA release following the field electrical stimulation not only acted through $GABA_A$Rs to suppress depolarizing responses but also activated $GABA_B$Rs to induce a long-lasting hyperpolarization mediated by GIRK channels, indicative of a pronounced $G_{i/o}$ component in the response of LS neurons to fi–fx fiber stimulation. Remarkably, both ATPD and hyperpolarization abolished AP firing (Fig. 1*B*). The pause duration, representing the sum of ATPD and hyperpolarization phases, was significantly longer in WT neurons than in *Trpc4*$^{-/-}$ neurons (Fig. 1*G*) due largely to the presence of ATPD (*SI Appendix*, Fig. S2*C*).

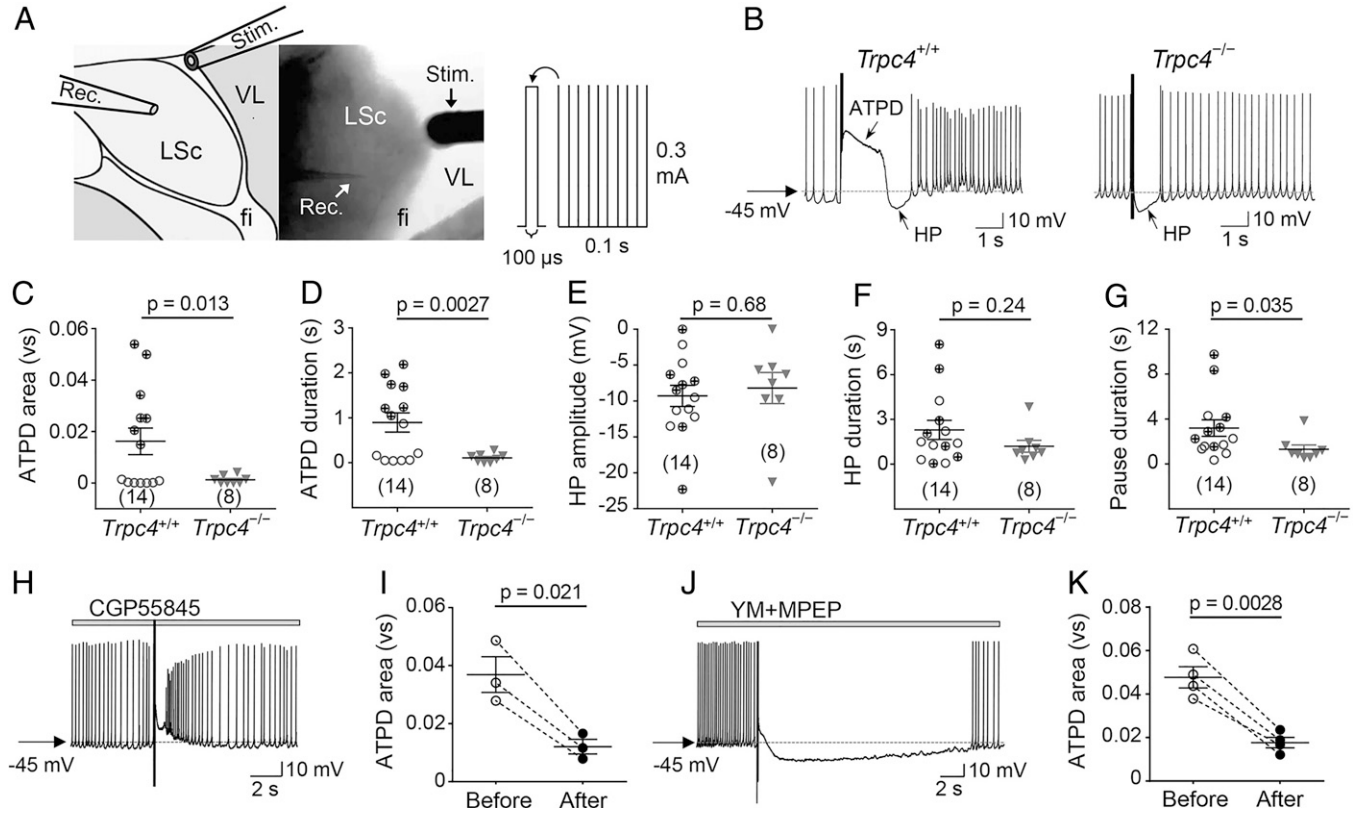

Fig. 1. Electrical stimulation of fi–fx fibers generates TRPC4-dependent plateau depolarization and TRPC4-independent hyperpolarization in LS neurons via metabotropic GABAR and glutamate receptor activation. (*A*) Diagram (*Left*) and microscopic picture (*Middle*) showing the electrical stimulation site and high-frequency burst stimulation protocol (*Right*); LSc, caudal part of the LS nucleus; VL, lateral ventricle; Stim., stimulating electrode; Rec., recording electrode. The stimulating burst was composed of 10 pulses (100 µs, 0.3 mA per pulse) at 100 Hz. (*B*) Representative traces of whole-cell current clamp recordings with baseline (prestimulus) potential adjusted to −45 mV for WT (*Trpc4*$^{+/+}$, *Left*) and TRPC4 knockout (*Trpc4*$^{-/-}$, *Right*) LS neurons. Note the appearance of ATPD followed by hyperpolarization (HP) in *Trpc4*$^{+/+}$ neurons. *Trpc4*$^{-/-}$ neurons only responded with a hyperpolarization. Fast neurotransmission was blocked with bicuculline (10 µM), CNQX (15 µM), and D-AP5 (30 µM). The perfusate also contained 4-AP (1 mM) and DHPG (1.3 µM), which facilitated the development of ATPD (*SI Appendix*, Fig. S1). (*C*–*G*) Statistics of ATPD area (*C*), ATPD duration (*D*), hyperpolarization amplitude (*E*), hyperpolarization duration (*F*), and total pause duration (*G*) for neurons recorded as in *B*. The "+" sign indicates neurons that developed ATPD. Horizontal bars are means ± SEM of cell numbers shown in parentheses. *P* values were determined by unpaired *t* test. (*H*) Representative trace recorded for a *Trpc4*$^{+/+}$ neuron as in *B*, but the perfusate additionally contained CGP55845 (20 µM) to block $GABA_B$Rs. (*I*) ATPD areas before and after the application of CGP55845 for individual neurons connected with dashed lines. Horizontal bars are means ± SEM, and *P* was determined by paired *t* test. (*J* and *K*) Similar to *H* and *I*, but YM298198 (YM; 30 µM) and MPEP (10 µM) were used to block mGluR1/5; mouse age, P21 to P49.

As with the previous study (10), ATPD and the corresponding large inward current were also successfully elicited in WT, but not in *Trpc4*$^{-/-}$, LS neurons by pairing the fi–fx fiber stimulation with step current injections (*SI Appendix*, Fig. S2 *D*–*G*). The step pulse was to provide a strong, brief depolarization that increases intracellular Ca^{2+} levels through voltage-gated Ca^{2+} channels (VGCCs). This Ca^{2+} signal triggers TRPC4 to enter a self-propagating mode of activation (6, 7), which underlies ATPD (10). As such, pairing the fi–fx fiber stimulation with an artificial depolarization induced ATPD in ∼82% (14/17) of WT neurons, and the lack of ATPD in *Trpc4*$^{-/-}$ neurons under these conditions validated its TRPC4 dependence (*SI Appendix*, Fig. S2*E*). However, the baseline potential of −80 mV precludes AP firing and is close to the K^+ equilibrium potential. To examine the effect of $G_{q/11}$–$G_{i/o}$ cotransmission on AP firing and GIRK-mediated hyperpolarization, we mainly analyzed recordings from −45-mV baseline potential without pairing by artificial depolarization, despite the lower success rate.

Interestingly, CGP55845 suppressed not only the hyperpolarization but also ATPD (Fig. 1 *H* and *I*), whereas inhibiting mGluR1/5 with YM298198 and 2-methyl-6-(phenylethynyl)-pyridine hydrochloride (MPEP) diminished ATPD but not hyperpolarization (Fig. 1 *J* and *K*). These drugs also suppressed the TRPC4-dependent inward currents in voltage clamp recordings (*SI Appendix*, Fig. S2 *H*–*K*). These data suggest that both $G_{q/11}$ and $G_{i/o}$, activated through mGluR1/5 and $GABA_B$Rs, respectively, contribute to the activation of endogenous TRPC4-containing channels in LS neurons in response to electrical stimulation of fi–fx fibers, consistent with TRPC4 being a coincidence detector of $G_{q/11}$ and $G_{i/o}$ signaling (6, 7).

Costimulation of $G_{q/11}$- and $G_{i/o}$-Coupled Receptors in LS Neurons Evokes ATPD Followed by Hyperpolarization. To mimic electrical stimulation–evoked responses, we applied DHPG and baclofen (a $GABA_B$R agonist) directly onto LS neurons (Fig. 2*A*). Consistent with mGluR1/5–$G_{q/11}$ coupling to cause excitation (25, 26) and $GABA_B$R–$G_{i/o}$ to cause inhibition (5, 27), 5 µM DHPG elicited BTD with a small depolarization (2.7 ± 0.5 mV, $n = 8$) and a clear acceleration of AP firing, which lasted for 5.6 ± 1.2 s before returning to the basal firing rate (Fig. 2*B*), whereas 30 µM baclofen evoked a strong (9.9 ± 0.8 mV, $n = 11$) and long-lasting (6.0 ± 0.9 s) hyperpolarization that abolished AP firing (Fig. 2*C*). However, with coapplication of DHPG and baclofen, ATPD emerged in 14 out of 29 neurons, with the plateau reaching −5.9 ± 1.7 mV ($n = 14$) and lasting for 1.62 ± 0.16 s, which was followed by a hyperpolarization (Fig. 2 *D*–*H*), reminiscent of the response

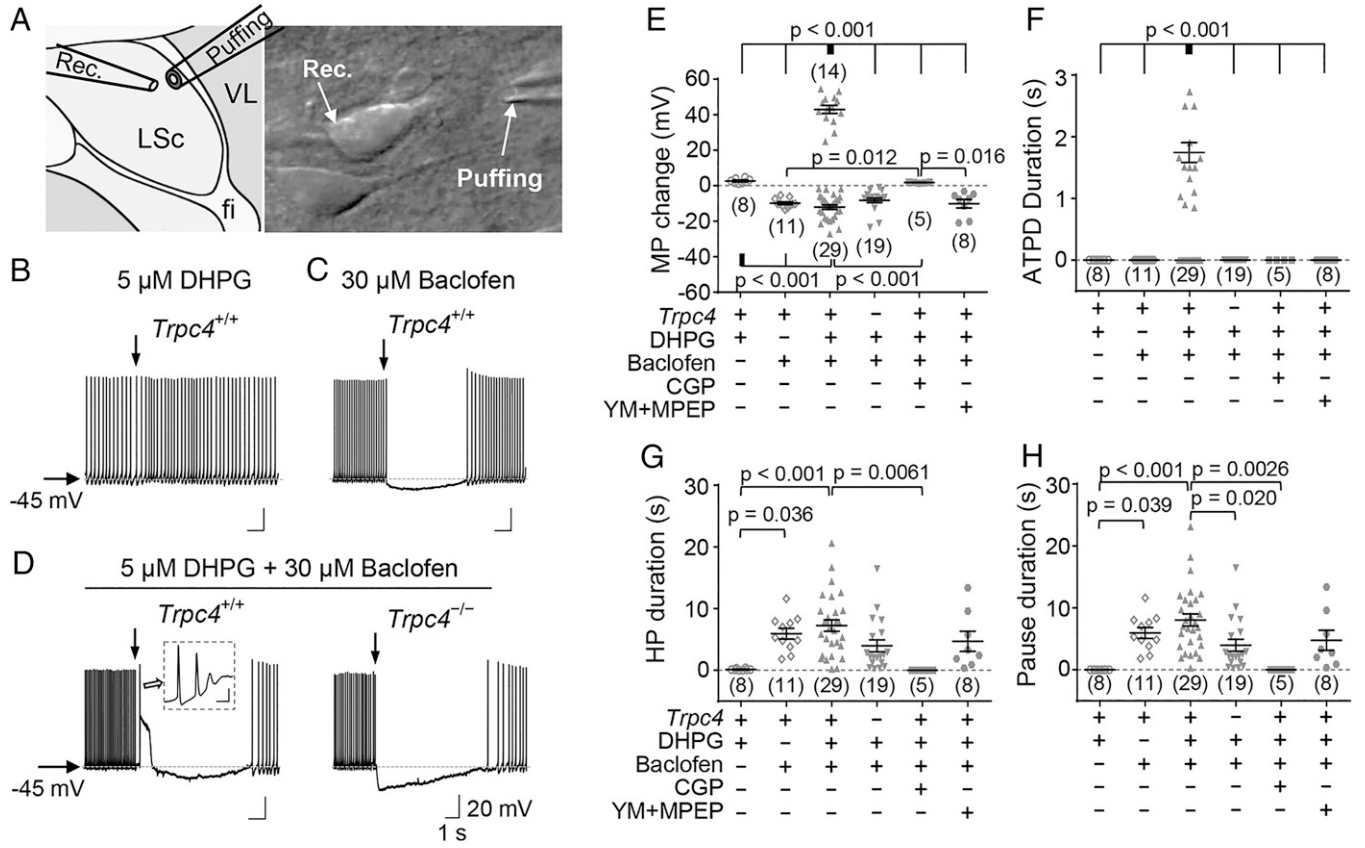

Fig. 2. Costimulation of group I mGluRs and $GABA_BRs$ in LS neurons evokes a robust TRPC4-dependent ATPD followed by an extended TRPC4-independent hyperpolarization. (*A*) Diagram for stimulation of LS neurons in brain slices by focal application of receptor agonists near soma and proximal dendrites via pressure ejection. Abbreviations are the same as in Fig. 1*A*. (*B–D*) Representative traces of whole-cell current clamp recordings with baseline potential adjusted to −45 mV for $Trpc4^{+/+}$ LS neurons that received ejection of 5 μM DHPG (*B*), 30 μM baclofen (*C*), or 5 μM DHPG plus 30 μM baclofen (*D*, *Left*). Drugs were ejected for 30 ms (5 to 30 psi) at the time point indicated by vertical arrows. Scale bars have the same values as marked in *D* (*Right*). Note the development of ATPD in $Trpc4^{+/+}$ neurons only when DHPG and baclofen were coapplied and the long hyperpolarization (~8 s) immediately after ATPD. *Inset*, expanded trace at the start of ATPD showing burst firing. (Scale bars, 5 ms, 20 mV.) However, coejection of DHPG and baclofen only caused hyperpolarization in $Trpc4^{-/-}$ neurons (*D*, *Right*). (*E–H*) Statistics of MP change (*E*), ATPD duration (*F*), hyperpolarization (HP) duration (*G*), and total pause duration (*H*) for neurons recorded as in *B* to *D* plus the effects of $GABA_BR$ antagonist CGP55845 (CGP; 20 μM) and mGluR1/5 antagonists YM298198 (YM; 30 μM) plus MPEP (10 μM) on the responses evoked by coejection of DHPG and baclofen. Horizontal bars are means ± SEM of cell numbers shown in parentheses. *P* values were determined by one-way ANOVA followed by Tukey's test; mouse age, P28 to P60.

elicited by stimulating the fi–fx fibers. When paired with current injection, ATPD and large inward currents also developed in current and voltage clamp recordings, respectively, in the majority of WT neurons that received both DHPG and baclofen (*SI Appendix*, Fig. S3).

Previously, we showed that ≥10 μM DHPG triggers not just BTD but also ATPD in LS neurons (10). Because DHPG has been reported to activate not only $G_{q/11}$ but also $G_{i/o}$ proteins in neurons (25, 28), we tested if $G_{i/o}$ proteins are involved in the DHPG-evoked ATPD by injecting PTX (0.1 μg/μL, 3 μL) bilaterally into the lateral ventricles, which are immediately next to the LS nuclei, 1 to 2 d before the recording. Not only did PTX completely eliminate the hyperpolarization induced by baclofen and by DHPG plus baclofen, it also abolished ATPD evoked by 30 μM DHPG as well as that by DHPG plus baclofen (Fig. 3). Thus, $G_{i/o}$ is activated by high concentrations of DHPG, and this is required for its induction of ATPD.

In addition to $G_{i/o}$, the lack of ATPD and large inward currents in $Trpc4^{-/-}$ neurons and in WT neurons in the presence of CGP55845 or YM298198 plus MPEP (Fig. 2 *D* and *F* and *SI Appendix*, Fig. S3) demonstrated their dependence on TRPC4 and coincident stimulation of $GABA_BRs$ and mGluR1/5. Also, similar to electrical stimulation–evoked responses, hyperpolarization was blocked by CGP55845 but not by YM298198 plus MPEP nor by deletion of TRPC4 (Fig. 2 *D*, *E*, and *G*). Furthermore, we were able to elicit ATPD in LS neurons by combining various receptor agonists known to trigger coincident $G_{i/o}$ and $G_{q/11}$ activation but not by selectively stimulating $G_{i/o}$ or $G_{q/11}$ alone (*SI Appendix*, Fig. S4 and Table S1), indicating that ATPD is commonly induced in LS neurons by costimulation of $G_{i/o}$ and $G_{q/11}$ signaling with respective neurotransmitters rather than being limited to mGluR1/5 or $GABA_BRs$.

The preceding data thus demonstrate that coincident stimulation of $G_{i/o}$ and $G_{q/11}$ signaling in LS neurons, either through synaptic transmission or direct focal application of $G_{i/o}$- and $G_{q/11}$-coupled receptor agonists, evokes membrane potential (MP) waveforms comprising a plateau depolarization followed by hyperpolarization. While the plateau depolarization results from $G_{q/11}$- and $G_{i/o}$-codependent activation of TRPC4, the hyperpolarization is due to $G_{i/o}$-mediated activation of GIRK channels. Both the plateau depolarization and hyperpolarization are long lasting, from ~1 s to tens of seconds, despite the very brief exposure to agonists (30 ms in focal ejection and 100 ms in electrical stimulation), and they suppress AP firing at permissive resting potentials (e.g., −45 mV).

Firing Patterns Reflect the Relative Strengths of $G_{q/11}$ and $G_{i/o}$ Inputs to LS Neurons. Remarkably, despite similar ATPD patterns (i.e., initial burst and robust plateau depolarization), the post-ATPD period exhibited large differences from cell to cell,

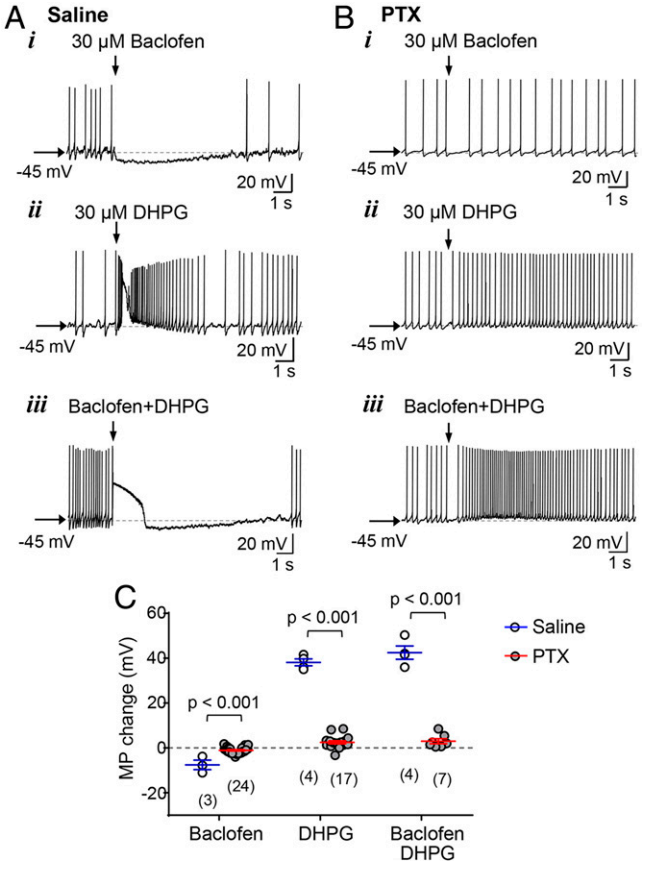

Fig. 3. $G\alpha_{i/o}$ dependence of strong TRPC4 activation (ATPD) in LS neurons. (*A* and *B*) Representative traces of whole-cell current clamp recordings of LS neurons in brain slices prepared from WT mice that received intraventricular injections of either saline (*A*) or PTX (0.3 μg/3 μL; *B*). The LS neurons were injected with a constant current to adjust their prestimulus potential to −45 mV and received pressure ejection of either 30 μM baclofen (*i*), 30 μM DHPG (*ii*), or 5 μM DHPG and 30 μM baclofen (*iii*) at the time point indicated by the downward arrow. Note that with the blockade of $G_{i/o}$ signaling by PTX, the hyperpolarization responses, reflective of GIRK channel activity, elicited by baclofen alone (*B*, *i*) and baclofen plus DHPG (*B*, *iii*) were no longer detected. More importantly, PTX blocked not only the induction of ATPD by baclofen plus DHPG (*B*, *iii*) but also that by 30 μM DHPG alone (*B*, *ii*), suggesting the involvement and critical role of $G_{i/o}$ signaling in ATPD induction (strong TRPC4 activation) when only DHPG (10 to 200 μM; see ref. 10) was applied. (*C*) Statistics of maximal MP changes (either depolarization or hyperpolarization) under the conditions in *A* and *B*. Horizontal bars are means ± SEM of cell numbers shown in the parentheses, with *P* values determined by unpaired *t* test; mouse age, P35 to P49.

especially with respect to the duration of hyperpolarization. Particularly when stimulated with 30 μM DHPG alone, most cells failed to show hyperpolarization. This resulted in two major differences from neurons that exhibited a hyperpolarization after ATPD. First, MP returned to baseline from a depolarized instead of a hyperpolarized potential, and second, AP firing resumed at a high frequency before slowing down to the basal or a new steady state (Fig. 4*A*), whereas with DHPG plus baclofen, ATPD converted to hyperpolarization, causing AP firing to resume at a low frequency before accelerating to the new steady state upon recovery of MP to baseline (Fig. 4*B*).

These data are consistent with relatively weak net activation of GIRK by 30 μM DHPG, which activates GIRK by weakly stimulating $G_{i/o}$ (25, 28) but also inhibits GIRK by stimulating $G_{q/11}$–PLC (3–5). To increase $G_{i/o}$ input, we coapplied baclofen (1 to 30 μM) with 30 μM DHPG. This resulted in a concentration-dependent increase in the overall pause duration (Fig. 4 *A* and *C*). Because the duration of ATPD was relatively constant under all conditions (Fig. 4 *A* and *D*), the elongated pauses mainly reflect the prolongation of hyperpolarization mediated by GIRK. Importantly, when the strength of $G_{i/o}$ was low, such as when no or 1 μM baclofen was applied, the hyperpolarization was undetected, and MP descended to baseline from ATPD to give rise to a decelerating AP firing pattern (Fig. 4*A*). The instantaneous firing rate (IFR) of APs during the recovery phase exhibited a decrease, as shown by the negative ΔIFR value (Fig. 4 *A* and *E*). However, when $G_{i/o}$ was strongly activated, as with >3 μM baclofen, the hyperpolarization outlasted ATPD, and, hence, during the recovery, MP ascended to baseline from a hyperpolarized level to produce an accelerating AP firing pattern, with ΔIFR having positive values (Fig. 4 *B* and *E*).

The above results suggest that information about the relative strengths of $G_{i/o}$ and $G_{q/11}$ inputs to LS neurons may be encoded by the combined activities of TRPC4 and GIRK. While the conductance of TRPC4 ($\bar{g}_{TRPC4}$) signifies coincident $G_{i/o}$–$G_{q/11}$ activation by producing ATPD, that of GIRK ($\bar{g}_{GIRK}$) reflects the relative strengths of the two G protein pathways by mediating hyperpolarization of varying durations. Consistent with this interpretation, both the amplitude and duration of hyperpolarization were also highly variable in neurons that developed ATPD in response to electrical stimulation of fi–fx fibers (Fig. 1 *E* and *F*). One of them even did not display obvious hyperpolarization (*SI Appendix*, Fig. S5*A*). As a result, AP firing recovered in a decelerating pattern, which is in stark contrast to the accelerating recovery pattern of neurons that exhibited hyperpolarization following ATPD (*SI Appendix*, Fig. S5*B*). Presumably, depending on the location of the LS neuron relative to the fi–fx pathway and its interconnectivity with neighboring LS neurons, the relative amounts of glutamate and GABA it received also varied, which would lead to different levels of GIRK activation.

Computer Simulations Reproduce the AP Firing Patterns Observed Experimentally with TRPC4 and GIRK Activated in Different Combinations. To verify that different combinations of TRPC4 and GIRK activation could produce the various AP firing patterns observed experimentally, we simulated neuronal responses in a conductance-based model neuron. Varying $\bar{g}_{TRPC4}$ and $\bar{g}_{GIRK}$ yielded firing patterns reminiscent of the experimental data (Fig. 5 *A* and *B*). We assumed that $\bar{g}_{TRPC4}$ and $\bar{g}_{GIRK}$ follow the relationships in which $G_{i/o}$ and $G_{q/11}$ cooperate to induce the strong self-propagating all-or-none activation of TRPC4, but they compete to stimulate GIRK, with the inhibition by $G_{q/11}$ being incomplete (Fig. 5*C*). Thus, $\bar{g}_{TRPC4}$ reaches the maximum in a range of $G_{i/o}$–$G_{q/11}$ inputs when either pathway was moderately (lowercase letters) to strongly (capital letters) activated. However, $\bar{g}_{GIRK}$ is at the maximum when $G_{i/o}$ is strongly active while $G_{q/11}$ is quiescent (0 in Fig. 5*C*). The five circled areas in Fig. 5*C* produced five distinctive patterns (P_1 to P_5, Fig. 5 *D* and *E* and *SI Appendix*, Fig. S6*A*), characterized by the presence or lack of a burst and/or a pause in AP firing as well as the way firing recovers after the pause. In P_1, $\bar{g}_{TRPC4}$ is low, and GIRK is inactive; AP firing increases without a burst or a pause, and the IFR recovers to the baseline by deceleration (Fig. 5 *D* and *E*, red). In P_2, $\bar{g}_{GIRK}$ is high, while $\bar{g}_{TRPC4}$ is low or zero; a pause occurs without a burst or an increase in IFR, and, after the pause, IFR recovers by acceleration (Fig. 5 *D* and *E*, orange). In P_3, $\bar{g}_{TRPC4}$ is high, while $\bar{g}_{GIRK}$ is low; a pause is preceded by a burst, and, after the pause, IFR recovers by deceleration (Fig. 5 *D* and *E*, cyan). In P_4, both $\bar{g}_{GIRK}$ and $\bar{g}_{TRPC4}$ are high; a pause is preceded by a burst, and, after the pause, IFR recovers by acceleration (Fig. 5 *D* and *E*, green). In P_5, $\bar{g}_{TRPC4}$ is low and $\bar{g}_{GIRK}$ is

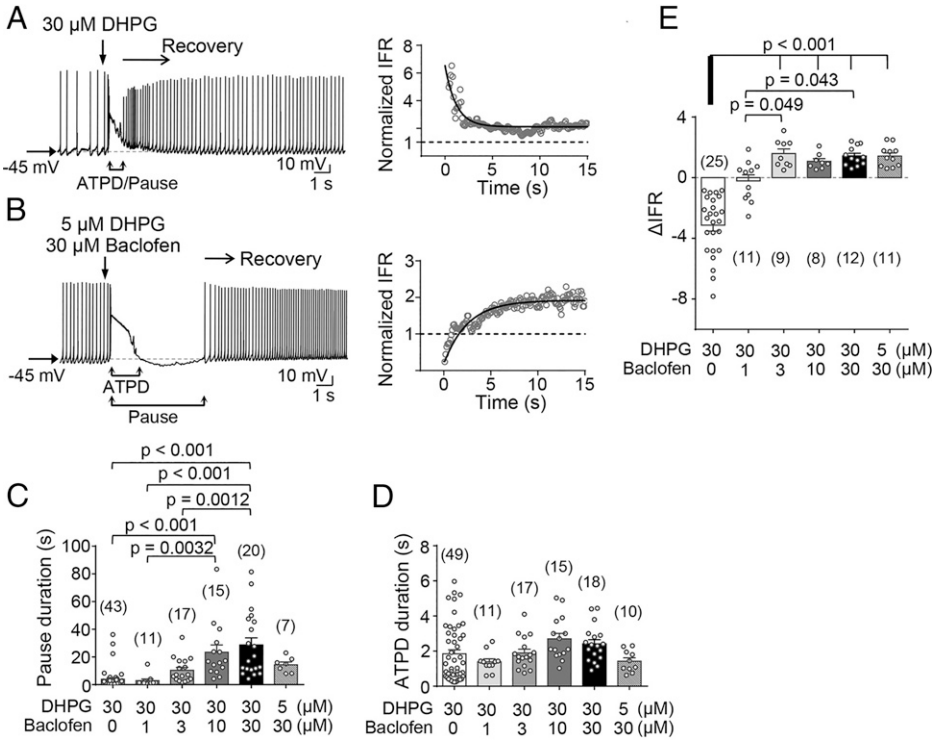

Fig. 4. The relative strength of $G_{q/11}$ and $G_{i/o}$ inputs to LS neurons is encoded as firing patterns. (*A* and *B*) Two distinct firing patterns recorded with baseline potential adjusted to −45 mV (*Left*) and the corresponding time courses of firing recovery (*Right*) of WT LS neurons that received ejection of 30 μM DHPG (*A*) or 5 μM DHPG plus 30 μM baclofen (*B*). Downward arrows indicate the time of drug ejection. Brackets below the trace show the periods of ATPD and total firing pause. Right-directed arrows indicate the start of firing recovery, from which IFR were normalized to the mean IFR of the same cell before the drug ejection (indicated by the dashed line and expressed as 1). The solid line is the exponential fit of the normalized IFR. (*C*–*E*) Comparisons of durations of firing pause (*C*) and ATPD (*D*) as well as magnitudes of IFR changes during firing recovery from the pause (*E*) of LS neurons that received combined stimulation of different concentrations of DHPG and baclofen. Pause (nonfiring period) duration (*C*) includes ATPD and hyperpolarization. Horizontal bars are means ± SEM of cell numbers shown in the parentheses, with *P* values determined by one-way ANOVA followed by Tukey's test; mouse age, P28 to P60.

moderate; IFR first increases and then decreases without displaying a burst or pause before recovering by acceleration (Fig. 5 *D* and *E*, gray, and *SI Appendix*, Fig. S6 *A* and *C*).

The pause duration, determined as the longest interspike interval (ISI), represents another important feature affected by the relative strengths of $\bar{g}_{TRPC4}$ and $\bar{g}_{GIRK}$, with higher $\bar{g}_{GIRK}$ generally leading to longer pauses (Fig. 5*F* and *SI Appendix*, Fig. S6*B*). However, the effect of $\bar{g}_{TRPC4}$ was biphasic depending on its ability to produce a depolarization block (i.e., ATPD). In the lower range, $\bar{g}_{TRPC4}$ antagonized the pause-extending effect of $\bar{g}_{GIRK}$, but above a threshold (2.5 to 3 depending on the level of $\bar{g}_{GIRK}$), an increase in $\bar{g}_{TRPC4}$ extended the pause duration (Fig. 5*F*).

In aggregate, the computational data support the idea that through coactivation of TRPC4 and GIRK channels, metabotropic neurotransmission mediated by $G_{q/11}$ and $G_{i/o}$ proteins can alter neuronal firing with distinctive patterns. Due to the differential effects of $G_{q/11}$ and $G_{i/o}$ on $\bar{g}_{TRPC4}$ and $\bar{g}_{GIRK}$ (Fig. 5*C*), these patterns encode information about the relative strengths of $G_{i/o}$ and $G_{q/11}$ inputs received by the postsynaptic neuron.

Discussion

Neurons receive transmitter inputs that act not only at ionotropic receptors but also at metabotropic receptors, which signal through G proteins, with $G_{q/11}$ and $G_{i/o}$ mediating excitatory and inhibitory effects, respectively (1, 2). However, our knowledge of how coincident $G_{i/o}$–$G_{q/11}$ inputs are processed remains incomplete, especially because the strengths of the two pathways are unlikely to be equal or kept at constant levels all the time. Given the diversity of neurotransmitters/neuromodulators and their corresponding metabotropic receptors, multiple G protein pathways are likely to be coactivated due to either converging inputs or the presence of multiple receptor types for the same transmitter (29). Thus, the ability to decipher the relative strengths of differential activations of two or more G protein pathways and faithfully convey the information downstream is pivotal.

Using the coincident $G_{q/11}$ and $G_{i/o}$ activation in LS neurons as an example, we show here that the relative strengths of $G_{i/o}$–$G_{q/11}$ inputs can be deciphered through TRPC4 and GIRK channels and encoded in AP firing patterns. While pure (or predominant) $G_{q/11}$ or $G_{i/o}$ input accelerates or shuts down firing, respectively, their coactivation can trigger a long pause of firing underscored by a strong depolarization that inactivates voltage-gated Na^+ channels without or with a subsequent hyperpolarization depending on the relative strengths of $G_{i/o}$ and $G_{q/11}$ inputs. The burst before the pause distinguishes the coincident $G_{i/o}$–$G_{q/11}$ inputs from $G_{i/o}$-only input, and the recovering patterns (deceleration versus acceleration and the rate) of AP firing after the pause, as well as the pause duration, reflect the relative strengths of $G_{i/o}$–$G_{q/11}$ inputs. Inevitably, these patterns can be further modified by other channels and signaling events, and the outcomes of individual neurons can differ greatly. For example, the MP waveform and hence the firing pattern may be further modulated due to $G_{i/o}$ regulation of VGCCs (30–32) and complex effects of PIP_2 on diverse ion channels, including many TRP channels (33–35), as well as from phosphorylation events associated with G protein

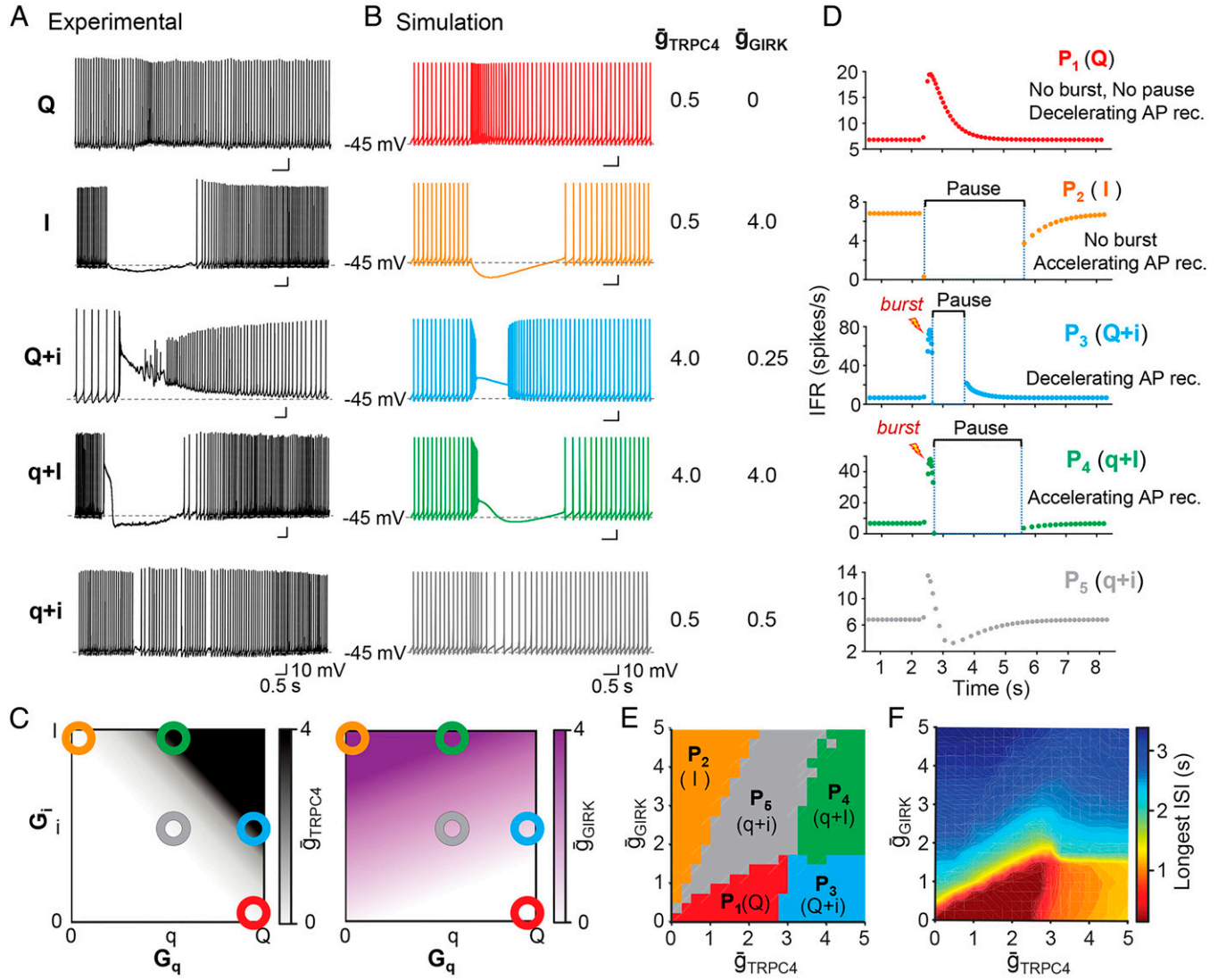

Fig. 5. Computational simulation replicates electrophysiological recordings of TRPC4- and GIRK-mediated MP waveforms and firing pattern changes. (*A*) Typical traces of whole-cell current clamp recordings with baseline potential adjusted to −45 mV from LS neurons representing the main classes of MP and firing pattern changes triggered by either pure (or predominant) $G_{q/11}$ (Q) or $G_{i/o}$ (I) stimulation or coincident $G_{q/11}$ and $G_{i/o}$ stimulations of varying strengths. For simplicity, capital and lowercase letters are used to represent strong and weak inputs, respectively. (*B*) Simulated firing patterns generated by varying TRPC4 and GIRK conductance densities ($\bar{g}_{TRPC4}$ and $\bar{g}_{GIRK}$ values indicated on the *Right* in mS/cm^2). (*C*) Hypothetical models depicting the effects of $G_{i/o}$–$G_{q/11}$ costimulation on $\bar{g}_{TRPC4}$ (*Left*) and $\bar{g}_{GIRK}$ (*Right*). Colored circles highlight conditions simulated in *B*. (*D*) IFR plotted against time for simulations in *B*, highlighting the distinctive patterns (P_1 to P_5) characterized by the presence or absence of a burst and a pause, pause duration, and IFR recovery patterns (decelerating versus accelerating). (*E*) Effect of $\bar{g}_{TRPC4}$ and $\bar{g}_{GIRK}$ on the simulated firing pattern. A 20-by-20 grid search was performed by varying $\bar{g}_{GIRK}$ and $\bar{g}_{TRPC4}$. The resulting patterns were classified using the same color code as in *B* to *D* into P_1 (red), P_2 (orange), P_3 (cyan), P_4 (green), and P_5 (gray) according to the classification scheme in *SI Appendix*, Fig. S6*A*. (*F*) Effect of $\bar{g}_{TRPC4}$ and $\bar{g}_{GIRK}$ on pause duration. For every combination of $\bar{g}_{GIRK}$ and $\bar{g}_{TRPC4}$ in *E*, IFR was plotted against time, and the longest ISI was plotted in the heat map.

signaling. Such effects would greatly enhance the flexibility and robustness of this information coding system. However, the core of this type of cellular information processing within a single postsynaptic neuron consists of minimally two channel types, TRPC4 and GIRK. Our computational model shows that different combinations of TRPC4 and GIRK are sufficient to reproduce the range of AP firing patterns observed experimentally, but it does not consider all the conductances that influence firing pattern in LS neurons nor does it simulate the underlying second messenger pathways controlling TRPC4 and GIRK activation. Future work may incorporate such details to better understand the consequences of comodulating TRPC4 and GIRK for information processing under more realistic conditions and to delineate the interactions between the underlying signaling pathways.

Both TRPC4 and GIRK are coregulated by $G_{q/11}$ and $G_{i/o}$ signaling but in different fashions (Fig. 5*C*). The activation of TRPC4 is dependent on $G_{i/o}$ through mainly $G\alpha_{i/o}$–GTP (36, 37), but GIRK is activated by $G\beta\gamma$ (3–5). In addition, while $G_{q/11}$–PLCβ signaling facilitates $G_{i/o}$ gating of TRPC4 by augmentation of Ca^{2+}- and H^+-dependent activation of PLCδ1 (6, 7), it antagonizes $G\beta\gamma$ activation of GIRK by hydrolyzing PIP_2 (3, 4). This also means that when TRPC4 is strongly active (e.g., during ATPD), GIRK is suppressed, as strong activation of TRPC4 involves a self-propagating interaction between TRPC4 and PLCδ1 (6, 7), and the latter keeps PIP_2 at low levels. For TRPC4 to enter the self-propagating activation mode, a strong Ca^{2+} signal is needed (6, 7), and in neurons, this triggering Ca^{2+} can arise from VGCCs (10, 38). As such, all forces known to enhance excitation or suppress

inhibition increase the probability of self-propagating activation of TRPC4. This explains why pairing the electrical stimulation with a positive current injection produced ATPD in the majority of LS neurons (*SI Appendix*, Fig. S2 *D* and *E*). Without the paired current injection, the depolarization relied solely on the excitation/inhibition balance the neuron received at the time of G protein stimulation. Thus, ATPD failed to develop when $GABA_A$Rs were active or fEPSP was blocked but resumed after further suppressing the inhibitory drive using 4-AP (*SI Appendix*, Fig. S1). Yet, the inhibitor mixture used could not guarantee that every neuron underwent depolarization necessary for VGCCs to provide sufficient triggering Ca^{2+} to initiate the self-propagating activation of TRPC4, which explains the lower success rate of ATPD induction (50%) when recorded at the baseline potential of −45 mV (Fig. 1 *B* and *C*). Interestingly, the inhibitory effect of the $GABA_B$R/GIRK pathway seemed to emerge rather slowly compared with TRPC4. This further illustrates the importance of $G_{q/11}$–PLCβ signaling, which, although not absolutely required, can greatly accelerate the rate of $G_{i/o}$-mediated TRPC4 activation (6, 7). Considering that $G_{q/11}$–PLCβ suppresses GIRK, during the initial phase of $G_{i/o}$–$G_{q/11}$ costimulation, $G_{q/11}$ allows TRPC4 to be activated before GIRK. The ensuing engagement of PLCδ1 (see above) then further suppresses GIRK until the self-propagating interaction between TRPC4 and PLCδ1 terminates. A number of factors could account for the termination of this self-propagating interaction and hence ATPD, including high micromolar Ca^{2+} concentrations and PIP_2 exhaustion (6) as well as increased inhibitory drive. Indeed, inhibiting 4-AP–sensitive K^+ channels extended ATPD (compare Fig. 1*C* and *SI Appendix*, Fig. S1*E*). However, exactly what regulates the duration of ATPD warrants further investigation.

Self-regeneration, all-or-nothing, and limited duration range are features also noted by researchers who originally characterized the ATPD-like phenomenon in LS neurons, which was referred to as epileptiform burst firing (11, 21, 22). We named it ATPD to emphasize the threshold dependence and self-regenerative nature of this response. ATPD-like responses, including the all-or-none feature, initial burst, and spike-shunting plateau potential, have also been reported in subthalamic neurons (39). By contrast, the activation of GIRK is graded, with its amplitude and duration under positive and negative regulation by $G_{i/o}$ and $G_{q/11}$ (and anything that activates PLC), respectively. Additionally, whereas GIRK causes hyperpolarization, TRPC4 induces depolarization that either accelerates or suppresses (via depolarization block of voltage-gated Na^+ channels) AP firing depending on the MP reached. Thus, there are multiple nonlinear interactions in this system that makes the outcome difficult to predict intuitively.

Our finding that TRPC4 and GIRK currents interact nonlinearly to produce distinctive AP firing patterns that reflect varying $G_{q/11}$ and $G_{i/o}$ combinations is significant from both encoding and decoding perspectives. For encoding, coincident $G_{q/11}$–$G_{i/o}$ inputs produce outputs that differ from the simple (linear) sum of inputs. The nonlinear interaction between TRPC4 and GIRK produces responses with qualitative differences depending on the input combination, which should be more robust than mere quantitative differences in terms of response distinctiveness and resilience to disruption by noise. For decoding, the combination of $G_{q/11}$–$G_{i/o}$ inputs received by a neuron could be inferred (decoded) from these distinctive responses. Although our results do not demonstrate how this affects the function of LS and their downstream neurons, the knowledge that specific $G_{i/o}$–$G_{q/11}$ combinations are translated into distinctive AP firing patterns improves understanding of the diverse firing patterns that have been described for various neurons.

Plateau potentials have long been observed in both vertebrate and invertebrate neurons, and their occurrence tends to be enhanced in the presence of G protein–coupled receptor agonist (40, 41). In most cases, plateau potentials do not cause depolarization block that precludes AP generation, and they have rarely been reported to depend on $G_{i/o}$. Therefore, ATPD may represent a special form of plateau potentials. More recent studies have implicated TRPC channels in some plateau potentials, which may also come in the form of slow EPSP and/or current (38, 42–45). In LS neurons, the TRPC4-dependent ATPD-like activity is responsible for the epileptiform burst firing that underlies pilocarpine-induced acute seizures and subsequent neuron death (9, 21). However, it is unlikely that this response pattern only exists under pathological conditions. Spontaneous ATPD-like events have been infrequently recorded from LS neurons in WT mouse brain slices in whole-cell current clamp without drug application or current injection (10, 11). They possess all the features and diversity as those shown in Fig. 5*A* and could reflect spontaneous costimulation of $G_{i/o}$ and $G_{q/11}$ pathways by endogenously released neurotransmitters. However, because of the strict requirement for coincident $G_{i/o}$–$G_{q/11}$ inputs and VGCC activation, these events are very rare in individual neurons, especially in brain slices in which network connectivity is compromised during slice preparation. Previously, cells displaying spontaneous ATPD-like events were referred to as "bursters", and it was reported that many "nonbursting" LS neurons could be converted into bursters by various receptor agonists, especially those of mGluR1/5 (11). More importantly, LS neuron bursting was completely abolished by treatment with PTX (11, 22). This is consistent with our observation that ATPD occurs in LS neurons exposed to receptor agonists known to coactivate $G_{i/o}$ and $G_{q/11}$ but not when $G_{q/11}$ or $G_{i/o}$ was activated alone (*SI Appendix*, Fig. S4 and Table S1). Thus, coincident activation of the $G_{q/11}$ and $G_{i/o}$ pathways represents a general mechanism that evokes robust activation of native TRPC4-containing channels that underlies ATPD irrespective of the specific transmitters and receptors involved.

LS neurons act as both local interneurons that communicate within the LS and as projection neurons that regulate activities in other areas of the septum and beyond (11). This makes it hard to predict what the overall network outcome would be based on the firing pattern responses to $G_{q/11}$–$G_{i/o}$ costimulation in single neurons. Nonetheless, the differential effects of coincident $G_{q/11}$–$G_{i/o}$ inputs on TRPC4 and GIRK channels shape MP waveforms in fashions that reflect the relative strengths of the two G protein pathways. Network connectivity to the LS neurons should then allow deciphering of the nature and intensities of neurochemical signals from different brain regions. Given that LS neurons receive diverse neurotransmitter inputs from many brain areas (11–13), the conversion of concurrent $G_{q/11}$ and $G_{i/o}$ signaling of differential strengths into discernible electrical responses by joint actions of TRPC4 and GIRK channels is vital for the lateral septum to serve as the information processing or relay center for higher-order brain functions, including, but not limited to, reward, feeding, anxiety, fear, sociability, memory, and locomotion (13, 14).

In summary, we uncover a previously unrecognized mechanism by which individual postsynaptic neurons encode information about the nature and relative strengths of coincident inputs triggering $G_{i/o}$ and $G_{q/11}$ signaling. This reporting

system uses a minimum of two channels, TRPC4 and GIRK, both of which are coregulated by $G_{i/o}$ and $G_{q/11}$ pathways. However, whereas the $G_{i/o}$ and $G_{q/11}$ pathways compete in their effects on GIRK, they cooperate in producing a self-propagating all-or-none activation of TRPC4. These nonlinear interactions allow for encoding of coincident signaling and more specifically the relative degrees to which the two G protein pathways are being activated by changing MP in defined fashions that yield discernible AP firing patterns. It is likely that this and similar mechanisms are widely used in the nervous system to transmit information about metabotropic signaling through G proteins.

Materials and Methods

Animals. WT and *Trpc4*$^{-/-}$ mice (both in the C57BL/6 background, postnatal day 21 (P21) to P60, male/female) were housed with free access to food and water under controlled light and temperature conditions. Mice were anesthetized by isoflurane before they were killed following procedures in accordance with NIH guidelines and approved by the Animal Welfare Committee of the University of Texas Health Science Center at Houston.

Brain Slice Preparation. Whole brains were excised and immediately immersed into ice-cold cutting solution consisting of 60 mM NaCl, 110 mM sucrose, 28 mM $NaHCO_3$, 7 mM $MgSO_4$, 3 mM KCl, 1.25 mM NaH_2PO_4, 0.5 mM $CaCl_2$, and 0.6 mM sodium ascorbate bubbled with 95% O_2 and 5% CO_2. The forebrain was blocked and mounted onto a prechilled cutting stage of a Leica VT1200S vibratome. Coronal slices (350 μm) were sectioned sequentially in the ice-cold cutting solution. Slices containing septal nuclei were transferred and incubated in normal artificial cerebrospinal fluid (aCSF) consisting of 125 mM NaCl, 26 mM $NaHCO_3$, 1 mM $MgSO_4$, 2.5 mM KCl, 1.25 mM NaH_2PO_4, 2 mM $CaCl_2$, and 10 mM glucose bubbled with 95% O_2 and 5% CO_2 at 35 °C for at least 90 min before recording.

Fi–Fx Stimulation. Fi–fx stimulation followed Joëls and Urban (46). A concentric electrode was positioned at the dorsolateral horn of the septum, where the hippocampal input enters the septum via the fimbria. Single train (10 pulses at 100 Hz, 100 μs/pulse, 0.3 to 1 mA) electrical stimulations were applied via the concentric electrode to the fi–fx fibers (Fig. 1*A*).

Drug Application. Drugs were diluted in aCSF and applied either through whole-chamber perfusion (for antagonists) or by pressure ejection through a drug delivery glass pipette positioned about 10 to 20 μm away from the target cell upstream of the aCSF flow (for agonists). The puffs were triggered and controlled by stimulation protocols programmed using PatchMaster software (HEKA Instruments). The puff duration was 30 ms, and the air pressure ranged between 5 and 30 psi. During the drug ejection, the recording chamber was continuously perfused with aCSF or aCSF containing the desired antagonists.

Patch Clamp Recordings. Glass pipettes (Sutter Instrument) were pulled using a Narishige PC-10 puller. The tip resistance was 3 to 6 MΩ when filled with intracellular solution, which contained 130 mM potassium methanesulfonate, 7 mM KCl, 0.05 mM ethylene glycol-bis(β-aminoethyl ether)-N,N,N′,N′-tetraacetic acid (EGTA), 1 mM Na_2-ATP, 3 mM Mg-ATP, 0.05 mM Na_2-GTP, and 10 mM 4-(2-hydroxyethyl)-1-piperazineethanesulfonic acid (HEPES), with pH 7.3 adjusted by KOH and osmolarity of 300 mOsm. LS neurons were visualized using a ×60 water objective lens connected with an infrared-differential interference contrast video microscope (Olympus BX51WI with OLY-150IR video camera). The LS neuron was voltage clamped at −70 mV when not being stimulated or tested. The temperature was maintained at ∼32 °C in the recording chamber by perfusion of aCSF preheated in an in-line heater (Warner Instrument) at 3 mL/min using a Rabbit peristaltic pump (Rainin Instrument).

For current clamp recordings reported in the main text, cells were adjusted to a baseline (prestimulus) potential of −45 mV to allow development of APs along with the observation of baseline MP changes over a long time period, typically 55 s. Fi–fx stimulation or drug ejection was applied after stable AP firing was detected. For some recordings (*SI Appendix*, Fig. S2 *A* and *B*), the starting potential was −70 mV for observation of MP changes without the interference of AP firing. To increase the chance of detecting ATPD, cells were also adjusted to a baseline potential of −80 mV, and a series of successive 20-ms, 200-pA current pulses with an interpulse interval of 1.3 s were applied immediately before the fi–fx stimulation (*SI Appendix*, Fig. S2 *D*, *Inset*) or a series of 20-ms current pulse injections from 200 pA to 1 nA with a 100-pA increment and an interpulse interval of 1.3 s were applied immediately before agonist ejection (*SI Appendix*, Fig. S3 *A*, *i*, *Inset*). This protocol was designed to allow coactivation of voltage-gated Ca^{2+}/Na^{+} channels in the recorded LS neurons to facilitate TRPC4 activation (10). For voltage clamp recordings, neurons were held at −70 mV, and step pulses to −45 mV for 50 ms and then −10 mV for 200 ms were applied to facilitate the development of TRPC4 current through activation of voltage-gated Ca^{2+}/Na^{+} channels (10). While fi–fx stimulation was initiated at the beginning of the −45-mV pulse (*SI Appendix*, Fig. S2 *F*, *Inset*), agonist ejection was triggered at the start of the −10 mV pulse (*SI Appendix*, Fig. S3 *B*, *i*, *Inset*). Recordings were made using an EPC10 amplifier controlled by PatchMaster software (both from HEKA). Data were acquired at 10 kHz and filtered at 3 kHz.

Simulation of Neuronal Firing. All simulations were conducted in MATLAB using the forward Euler integration method and a time step of 0.01. All code is available at http://modeldb.yale.edu/267363 and at http://prescottlab.ca/code-for-models. We used the modified Morris–Lecar model (38):

$$C\frac{dV}{dt} = -g_{\text{leak}}(V - E_{\text{leak}}) - \bar{g}_{\text{Na}}m_{\infty}(V)h n(V - E_{\text{Na}}) - \bar{g}_{\text{K}}w(V - E_{\text{K}})$$
$$-\bar{g}_{\text{AHP}}a(V - E_{\text{K}}) - \bar{g}_{\text{Ca}}b(V - E_{\text{Ca}}) - \bar{g}_{\text{TRPC4}}z_{\infty}(\text{Ca})(V - E_{\text{CAN}})$$
$$-\bar{g}_{\text{GIRK}}q(V - E_{\text{K}})$$

where all parameters were kept the same as ref. 38 except as follows: $\bar{g}_{\text{AHP}} = 10$ mS/cm^2, $\bar{g}_{\text{Ca}} = 0.02$ mS/cm^2, $\beta_w = 5$ mV, $\gamma_h = -8$ mV, $\beta_h = -27$ mV, $\beta_n = -25$ mV, $\varphi_h = 0.03$, $\gamma_n = -5$ mV, $\varphi_n = 10$, and $E_{\text{leak}} = -50$ mV. Fast (h) and slow (n) sodium inactivation from Rho and Prescott (47) were added to facilitate complete sodium channel inactivation. GIRK channel from Yim et al. (48) was modified to match experimental current-voltage curve (49):

$$q_{\infty} = \frac{1}{1 + e^{\frac{V - V_{0.5}}{kl}}} + \frac{0.8}{1 + e^{\frac{V - V_{0.5}}{100}}}$$

The second term was added to allow sustained outward current at depolarized potentials above −20 mV. A built-in NEURON function Exp2Syn was used to simulate slow rise and decay of $\bar{g}_{\text{GIRK}}$ and $\bar{g}_{\text{TRPC}}$ in EPSP-like waveforms. The rise time constant (τ_{rise}) of $\bar{g}_{\text{TRPC4}}$ was set to be shorter than that of $\bar{g}_{\text{GIRK}}$ to recapitulate pattern 4 (q + I), where sustained hyperpolarization is preceded by a short ATPD.

Data Analysis. Several parameters that reflect the waveform characters of the plateau depolarization (ATPD), hyperpolarization, and inward current, including MP change (amplitude of ATPD or hyperpolarization), ATPD area under the trace (AUC), ATPD duration, hyperpolarization duration, duration of pause of firing, as well as the amplitudes of peak current, were measured and used for quantitative analysis of the response patterns. The maximal amplitudes of ATPD, BTD, hyperpolarization, and inward current were measured at the point where maximal depolarization, hyperpolarization, or inward current reached its first peak following electrical or drug stimulation, excluding all APs. The duration of ATPD or hyperpolarization was measured between the initial point when MP deviated markedly from baseline for at least 10 consecutive data points in the same direction and the point where the MP recovered to generate the first AP or first crossed the holding potential (Fig. 4 *A* and *B*). The AUC was measured as the integral of individual data points of MP increase over the holding potential between the first point following electrical/drug stimulation and the point where MP recovered to the holding potential or the last recorded point if the MP did not recover to the holding potential (*SI Appendix*, Fig. S2*D*). If multiple ATPDs were detected in a single neuron, the one with the greatest AUC value was used for analysis. The pause of firing was the combination of both ATPD and hyperpolarization durations or just the ATPD or hyperpolarization duration if only one of these emerged.

IFR of APs was calculated to represent the changes of firing patterns. IFR is the reciprocal of ISI measured between sequential APs. IFR values were calculated for APs during the recovery phase of AP firing after the pause caused by

ATPD or hyperpolarization. Fitting the IFR values with an exponential function gave rise to the time constant (τ). ΔIFR was calculated by subtraction of the first IFR in the recovery phase from the new steady-state IFR reached by the neuron.

Statistical Analysis. A Student's *t* test was used to compare the mean value differences between two groups. ANOVA followed by post hoc tests were used to compare differences among three or more groups. Differences were considered significant if at least $P < 0.05$. All data values in text and figures are presented as means ± SEM.

Data Availability. All study data are included in the article and/or *SI Appendix*.

ACKNOWLEDGMENTS. We thank Dr. Marc Freichel (Heidelberg University) for *Trpc4*$^{-/-}$ mice. This work was funded by NIH grants R01NS092377 and R01NS102452 (to M.X.Z.), NIH Intramural Research Program Projects Z01-ES-101684 and Z01-ES-101643 (to L.B.), Deutsche Forschungsgemeinschaft Collaboration Research Centre TRR 152, project P01 (to V.F.), Hospital for Sick Children Restracomp Award (to J.Y.), and Canadian Institutes of Health Research Foundation Grant FDN-167276 (to S.A.P.).

Author affiliations: [a]Department of Integrative Biology and Pharmacology, McGovern Medical School, The University of Texas Health Science Center at Houston, Houston, TX 77030; [b]Neurosciences & Mental Health, The Hospital for Sick Children, Toronto, ON M5G 0A4, Canada; [c]Institute of Biomedical Engineering, University of Toronto, Toronto, ON M5S 3G9, Canada; [d]Experimental and Clinical Pharmacology and Toxicology, Saarland University, Homburg, 66421, Germany; [e]Department of Physiology, University of Toronto, Toronto, ON M5S 1A8, Canada; [f]Institute for Biomedical Research (BIOMED UCA-CONICET), School of Medical Sciences, Catholic University of Argentina (UCA), Buenos Aires, C1107AFF, Argentina; and [g]Signal Transduction Laboratory, National Institute of Environmental Health Sciences, Research Triangle Park, NC 27709

1. K. M. Betke, C. A. Wells, H. E. Hamm, GPCR mediated regulation of synaptic transmission. *Prog. Neurobiol.* **96**, 304–321 (2012).
2. J. S. Wiegert, M. Mahn, M. Prigge, Y. Printz, O. Yizhar, Silencing neurons: Tools, applications, and experimental constraints. *Neuron* **95**, 504–529 (2017).
3. C. L. Huang, S. Feng, D. W. Hilgemann, Direct activation of inward rectifier potassium channels by PIP2 and its stabilization by G$\beta\gamma$. *Nature* **391**, 803–806 (1998).
4. H. Zhang, C. He, X. Yan, T. Mirshahi, D. E. Logothetis, Activation of inwardly rectifying K^+ channels by distinct PtdIns(4,5)P_2 interactions. *Nat. Cell Biol.* **1**, 183–188 (1999).
5. C. Lüscher, P. A. Slesinger, Emerging roles for G protein-gated inwardly rectifying potassium (GIRK) channels in health and disease. *Nat. Rev. Neurosci.* **11**, 301–315 (2010).
6. D. P. Thakur *et al.*, Critical roles of $G_{i/o}$ proteins and phospholipase C-δ1 in the activation of receptor-operated TRPC4 channels. *Proc. Natl. Acad. Sci. U.S.A.* **113**, 1092–1097 (2016).
7. D. P. Thakur, Q. Wang, J. Jeon, J. B. Tian, M. X. Zhu, Intracellular acidification facilitates receptor-operated TRPC4 activation through PLCδ1 in a Ca^{2+}-dependent manner. *J. Physiol.* **598**, 2651–2667 (2020).
8. H. Wang *et al.*, TRPC channels: Structure, function, regulation and recent advances in small molecular probes. *Pharmacol. Ther.* **209**, 107497 (2020).
9. K. D. Phelan *et al.*, Heteromeric canonical transient receptor potential 1 and 4 channels play a critical role in epileptiform burst firing and seizure-induced neurodegeneration. *Mol. Pharmacol.* **81**, 384–392 (2012).
10. J. Tian *et al.*, Dual depolarization responses generated within the same lateral septal neurons by TRPC4-containing channels. *Pflugers Arch.* **466**, 1301–1316 (2014).
11. J. P. Gallagher, F. Zheng, H. Hasuo, P. Shinnick-Gallagher, Activities of neurons within the rat dorsolateral septal nucleus (DLSN). *Prog. Neurobiol.* **45**, 373–395 (1995).
12. T. P. Sheehan, R. A. Chambers, D. S. Russell, Regulation of affect by the lateral septum: Implications for neuropsychiatry. *Brain Res. Brain Res. Rev.* **46**, 71–117 (2004).
13. C. A. Rizzi-Wise, D. V. Wang, Putting together pieces of the lateral septum: Multifaceted functions and its neural pathways. *eNeuro* **8**, ENEURO.0315-21.2021 (2021).
14. H. S. Wirtshafter, M. A. Wilson, Lateral septum as a nexus for mood, motivation, and movement. *Neurosci. Biobehav. Rev.* **126**, 544–559 (2021).
15. P. Y. Risold, L. W. Swanson, Chemoarchitecture of the rat lateral septal nucleus. *Brain Res. Brain Res. Rev.* **24**, 91–113 (1997).
16. N. Holderith, F. Varoqueaux, Z. Borhegyi, C. Leranth, Dual (excitatory and inhibitory) calretinin innervation of AMPA receptor-containing neurons in the rat lateral septum. *Exp. Brain Res.* **119**, 65–72 (1998).
17. M. A. Fowler, K. Sidiropoulou, E. D. Ozkan, C. W. Phillips, D. C. Cooper, Corticolimbic expression of TRPC4 and TRPC5 channels in the rodent brain. *PLoS One* **2**, e573 (2007).
18. J. F. DeFrance, T. Shimono, S. T. Kitai, Hippocampal inputs to the lateral septal nucleus: Patterns of facilitation and inhibition. *Brain Res.* **37**, 333–339 (1972).
19. P. Y. Risold, L. W. Swanson, Connections of the rat lateral septal complex. *Brain Res. Brain Res. Rev.* **24**, 115–195 (1997).
20. C. Chaichim, M. J. Radnan, G. Dumlao, J. M. Power, Long-term depression of excitatory transmission in the lateral septum. *J. Neurophysiol.* **125**, 1825–1832 (2021).
21. F. Zheng, K. D. Phelan, The role of canonical transient receptor potential channels in seizure and excitotoxicity. *Cells* **3**, 288–303 (2014).
22. F. Zheng, H. Hasuo, J. P. Gallagher, 1*S*,3*R*-ACPD-preferring inward current in rat dorsolateral septal neurons is mediated by a novel excitatory amino acid receptor. *Neuropharmacology* **34**, 905–917 (1995).
23. M. Raggenbass, P. Pierson, D. Metzger, S. Alberi, Action of a metabotropic glutamate receptor agonist in rat lateral septum: Induction of a sodium-dependent inward aftercurrent. *Brain Res.* **776**, 75–87 (1997).
24. H. Hasuo, T. Akasu, Activation of inhibitory pathways suppresses the induction of long-term potentiation in neurons of the rat lateral septal nucleus. *Neuroscience* **105**, 343–352 (2001).
25. E. Hermans, R. A. Challiss, Structural, signalling and regulatory properties of the group I metabotropic glutamate receptors: Prototypic family C G-protein-coupled receptors. *Biochem. J.* **359**, 465–484 (2001).
26. C. M. Niswender, P. J. Conn, Metabotropic glutamate receptors: Physiology, pharmacology, and disease. *Annu. Rev. Pharmacol. Toxicol.* **50**, 295–322 (2010).
27. A. Pinard, R. Seddik, B. Bettler, $GABA_B$ receptors: Physiological functions and mechanisms of diversity. *Adv. Pharmacol.* **58**, 231–255 (2010).
28. T. A. Kreibich, S. H. Chalasani, J. A. Raper, The neurotransmitter glutamate reduces axonal responsiveness to multiple repellents through the activation of metabotropic glutamate receptor 1. *J. Neurosci.* **24**, 7085–7095 (2004).
29. M. P. Nusbaum, D. M. Blitz, E. Marder, Functional consequences of neuropeptide and small-molecule co-transmission. *Nat. Rev. Neurosci.* **18**, 389–403 (2017).
30. L. Birnbaumer *et al.*, Molecular diversity and function of G proteins and calcium channels. *Biol. Reprod.* **44**, 207–224 (1991).
31. N. Qin, D. Platano, R. Olcese, E. Stefani, L. Birnbaumer, Direct interaction of G$\beta\gamma$ with a C-terminal G$\beta\gamma$-binding domain of the Ca^{2+} channel α1 subunit is responsible for channel inhibition by G protein-coupled receptors. *Proc. Natl. Acad. Sci. U.S.A.* **94**, 8866–8871 (1997).
32. G. W. Zamponi, K. P. Currie, Regulation of Ca_V2 calcium channels by G protein coupled receptors. *Biochim. Biophys. Acta* **1828**, 1629–1643 (2013).
33. B. Nilius *et al.*, The Ca^{2+}-activated cation channel TRPM4 is regulated by phosphatidylinositol 4,5-biphosphate. *EMBO J.* **25**, 467–478 (2006).
34. T. Voets, B. Nilius, Modulation of TRPs by PIPs. *J. Physiol.* **582**, 939–944 (2007).
35. T. Rohacs, Phosphoinositide regulation of TRP channels. *Handb. Exp. Pharmacol.* **223**, 1143–1176 (2014).
36. J. P. Jeon *et al.*, Selective Gα_i subunits as novel direct activators of transient receptor potential canonical (TRPC)4 and TRPC5 channels. *J. Biol. Chem.* **287**, 17029–17039 (2012).
37. J. P. Jeon, D. P. Thakur, J. B. Tian, I. So, M. X. Zhu, Regulator of G-protein signalling and GoLoco proteins suppress TRPC4 channel function via acting at $G\alpha_{i/o}$. *Biochem. J.* **473**, 1379–1390 (2016).
38. S. Ratté, S. Karnup, S. A. Prescott, Nonlinear relationship between spike-dependent calcium influx and TRPC channel activation enables robust persistent spiking in neurons of the anterior cingulate cortex. *J. Neurosci.* **38**, 1788–1801 (2018).
39. J. I. Kass, I. M. Mintz, Silent plateau potentials, rhythmic bursts, and pacemaker firing: Three patterns of activity that coexist in quadristable subthalamic neurons. *Proc. Natl. Acad. Sci. U.S.A.* **103**, 183–188 (2006).
40. E. Marder, R. L. Calabrese, Principles of rhythmic motor pattern generation. *Physiol. Rev.* **76**, 687–717 (1996).
41. D. Derjean *et al.*, Dynamic balance of metabotropic inputs causes dorsal horn neurons to switch functional states. *Nat. Neurosci.* **6**, 274–281 (2003).
42. J. Hartmann *et al.*, TRPC3 channels are required for synaptic transmission and motor coordination. *Neuron* **59**, 392–398 (2008).
43. C. Tai, D. J. Hines, H. B. Choi, B. A. MacVicar, Plasma membrane insertion of TRPC5 channels contributes to the cholinergic plateau potential in hippocampal CA1 pyramidal neurons. *Hippocampus* **21**, 958–967 (2011).
44. A. Riccio *et al.*, Decreased anxiety-like behavior and $G\alpha_{q/11}$-dependent responses in the amygdala of mice lacking TRPC4 channels. *J. Neurosci.* **34**, 3653–3667 (2014).
45. J. Bröker-Lai *et al.*, Heteromeric channels formed by TRPC1, TRPC4 and TRPC5 define hippocampal synaptic transmission and working memory. *EMBO J.* **36**, 2770–2789 (2017).
46. M. Joëls, I. J. Urban, Topographic organization of fimbria-fornix fibers projecting to the lateral septum of rats: A single and field response analysis. *Exp. Neurol.* **87**, 474–486 (1985).
47. Y.-A. Rho, S. A. Prescott, Identification of molecular pathologies sufficient to cause neuropathic excitability in primary somatosensory afferents using dynamical systems theory. *PLoS Comput. Biol.* **8**, e1002524 (2012).
48. M. Y. Yim, A. Hanuschkin, J. Wolfart, Intrinsic rescaling of granule cells restores pattern separation ability of a dentate gyrus network model during epileptic hyperexcitability. *Hippocampus* **25**, 297–308 (2015).
49. L. G. Hommers, M. J. Lohse, M. Bünemann, Regulation of the inward rectifying properties of G-protein-activated inwardly rectifying K^+ (GIRK) channels by G$\beta\gamma$ subunits. *J. Biol. Chem.* **278**, 1037–1043 (2003).